Climate Dynamics (2002) 19: 181–190
DOI 10.1007/s00382-001-0216-6

R.M. Ponte · J. Rajamony · J.M. Gregory

Ocean angular momentum signals in a climate model and implications for Earth rotation

Received: 22 June 2001 / Accepted: 26 November 2001 / Published online: 9 March 2002

Abstract Estimates of ocean angular momentum (OAM) provide an integrated measure of variability in ocean circulation and mass fields and can be directly related to observed changes in Earth rotation. We use output from a climate model to calculate 240 years of 3-monthly OAM values (two equatorial terms L_1 and L_2, related to polar motion or wobble, and axial term L_3, related to length of day variations) representing the period 1860–2100. Control and forced runs permit the study of the effects of natural and anthropogenically forced climate variability on OAM. All OAM components exhibit a clear annual cycle, with large decadal modulations in amplitude, and also longer period fluctuations, all associated with natural climate variability in the model. Anthropogenically induced signals, inferred from the differences between forced and control runs, include an upward trend in L_3, related to inhomogeneous ocean warming and increases in the transport of the Antarctic Circumpolar Current, and a significantly weaker seasonal cycle in L_2 in the second half of the record, related primarily to changes in seasonal bottom pressure variability in the Southern Ocean and North Pacific. Variability in mass fields is in general more important to OAM signals than changes in circulation at the seasonal and longer periods analyzed. Relation of OAM signals to changes in surface atmospheric forcing are discussed. The important role of the oceans as an excitation source for the annual, Chandler and Markowitz wobbles, is confirmed. Natural climate variability in OAM and related excitation is likely to measurably affect the Earth rotation, but anthropogenically induced effects are comparatively weak.

R.M. Ponte (✉) · J. Rajamony
Atmospheric and Environmental Research, Inc., 131 Hartwell Avenue, Lexington, MA 02421-3126, USA
E-mail: ponte@aer.com

J.M. Gregory
Hadley Centre, Meteorological Office, London Road, Bracknell, Berkshire, United Kingdom RG12 2SY

1 Introduction

Basic conservation principles require that the total angular momentum of the Earth, including its fluid envelope, remains a constant in the absence of external torques on the planet, which is essentially true if one excludes the effects of tidal braking on the Earth–Moon system (Munk and MacDonald 1960; Lambeck 1980). The two rotating geophysical fluids, ocean and atmosphere, continuously exchange angular momentum with the solid Earth and thus excite motions of the Earth's axis of rotation with respect to the crust or polar motion (PM) and changes in the Earth's rate of rotation or length of day (LOD). Climate variability in the ocean–atmosphere system and Earth rotation signals can thus be closely linked.

Long records of global atmospheric angular momentum (AAM) have allowed extensive study of its seasonal and lower frequency variability in relation to atmospheric circulation and climate (Hide et al. 1997; Rosen and Salstein 2000) and to Earth rotation changes (Hide and Dickey 1991; Rosen 1993; Eubanks 1993). Besides the well-established link among the subtropical jet streams (and, hence, AAM) and LOD on seasonal time scales, climate signals such as El Niño and the Quasi-Biennial Oscillation have a clear impact on AAM and LOD (Rosen et al. 1984; Abarca del Rio et al. 2000). Influence of the North Atlantic Oscillation on AAM and PM has also been noted (Chao and Zhou 1999). Long Earth rotation records can thus serve as a proxy for AAM (Salstein and Rosen 1986), and in turn AAM can serve as a useful global index of the atmospheric state under past and future climate scenarios (Rosen and Gutowski 1992; Rosen and Salstein 2000; Huang et al. 2001).

Similar studies of ocean angular momentum (OAM) have been hampered by the lack of long records, but recent work also indicates a clear connection among ocean circulation changes, OAM, and Earth rotation. The role of OAM in PM excitation at seasonal and Chandler (~14 month) periods was demonstrated by Ponte et al. (1998) and Ponte and Stammer (1999) and further confirmed by Wünsch (2000), Gross (2000a), and Brzeziński and Nastula (2001), using 11+ years of global ocean model output. Celaya et al. (1999) extended the results to longer time scales based on 120 years of OAM output from a climate model and probed the role of the ocean in the ~30-year Markowitz wobble as well. Marcus et al. (1998) and Ponte and Stammer (2000) found measurable but weak oceanic influence on LOD at seasonal time scales. The seasonal signals in OAM have been traced to changes in the oceanic gyre and circumpolar circulation and mass fields (Ponte and Stammer 1999, 2000).

In the present work, we examine OAM seasonal and lower frequency variability based on 240 years of output from the Hadley Centre coupled climate model, version HadCM2 (Johns et al. 1997). Ocean model output from two HadCM2 runs is used: a "control" run, which simulates the current climate under present levels of greenhouse gases, and a "forced" run, which simulates an anthropogenically influenced climate-change scenario, forced with estimates of historical and future increases of greenhouse gases and sulfate aerosols. Our analysis extends recent OAM studies in several ways. Results from the control and forced runs permit one to address not only how natural climate variability affects OAM, but also how OAM may vary under anthropogenic climate forcing, as done for AAM by Rosen and Gutowski (1992) and Huang et al. (2001). Our analysis attempts to relate OAM low frequency signals to regional changes in the currents, density, and sea level fields, and thus sheds light on the potential use of OAM as a global index of climate variability in the ocean circulation and mass fields. In addition, with a substantially longer time series than previously examined, we can further clarify possible links between OAM changes and Earth rotation signals such as the Chandler and Markowitz wobbles.

2 Model output and calculations

The OAM vector can be broken into three components: L_1 and L_2, about the equatorial axes pointing to 0° and 90°E meridians, respectively, and related to excitation of PM; and L_3, about Earth's polar axis, and related to LOD changes. Each component consists of a matter term, due to solid body rotation and dependent on bottom pressure fields, and a motion term, due to velocities relative to solid body rotation. Matter and motion terms are denoted here by P and V, respectively, and given by

$$(P_1,P_2) = -\frac{\Omega r^4}{g}\int\int p_b \sin\phi\cos^2\phi(\cos\lambda,\sin\lambda)\mathrm{d}\phi\,\mathrm{d}\lambda \tag{1}$$

$$(V_1,V_2) = -r^3\rho_o\int\int[u\sin\phi\cos\phi(\cos\lambda,\sin\lambda) + v\cos\phi(-\sin\lambda,\cos\lambda)]\mathrm{d}\phi\,\mathrm{d}\lambda \tag{2}$$

$$P_3 = \frac{\Omega r^4}{g}\int\int p_b\cos^3\phi\,\mathrm{d}\phi\,\mathrm{d}\lambda \tag{3}$$

$$V_3 = r^3\rho_o\int\int u\cos^2\phi\,\mathrm{d}\phi\,\mathrm{d}\lambda \tag{4}$$

where ϕ and λ are the latitude and longitude, r is the radius and Ω is the rotation rate of the Earth, u and v are the vertically integrated zonal and meridional currents, p_b is the ocean bottom pressure, ρ_o is the mean ocean density, and g is the acceleration of gravity. Quantities in Eqs. (1)–(4) can denote local or global OAM values depending on the surface area considered in the integrals.

Our estimates of the OAM integrals are based on output from the HadCM2 runs described in detail by Mitchell et al. (1995). For brevity, only pertinent issues are briefly revisited here. The coupled HadCM2 model (Johns et al. 1997) was run for 240 years representing the period from 1860 to 2100, under "control" and "forced" cases, where the forcing for the latter consists of historical greenhouse gas (represented as equivalent CO_2) and sulfate aerosol concentrations until 1990, after which the concentrations increase following scenario IS92a (Houghton et al. 1992). For the control run, forcing is held constant. The climate variability simulated in the HadCM2 runs is fairly realistic (Tett et al. 1997; Collins 2000). Values of OAM are calculated four times a year from pressure and velocity data averaged over three-month periods and given on a 3.75° longitude by 2.5° latitude grid.

For this rigid-lid model, the total ocean bottom pressure, p_b, is given by the sum of p_ρ, which is the pressure due to the integral of density ρ over the water column, and p_s, which is the pressure on the rigid lid due to dynamic surface signals. Values of p_s are estimated as in Gregory and Lowe (2000). Spatial gradients of p_s are diagnosed from the prognostic model variables, and values of p_s are then determined to within a spatial constant by a minimization method, as described in detail by Gregory (1993). The undetermined constant is related to globally averaged mean sea level changes and corresponding variations in ocean volume that must also be inferred. Note that the model formulation of the continuity equation and the rigid lid imply conservation of volume, and thus changes in density are not accounted for by changes in volume. For example, a uniform warming of the global ocean, which in reality implies no change in mass, would induce a decrease in p_b through a decrease in p_ρ in the model, because the water column lightens. The unmodeled volume changes can, nevertheless, be accounted for by assuming that they translate into a spatially homogeneous sea level correction (Ponte 1999; Greatbatch 1994; Gregory 1993) given by

$$\text{Sea level correction} = -\frac{1}{A}\int\frac{\delta\rho}{\rho_o}\,\mathrm{d}V = -\frac{1}{A}\int\int\frac{\delta\rho}{\rho_o}\,\mathrm{d}z\,\mathrm{d}A = -\frac{1}{A}\int\frac{\delta p_\rho}{g\rho_o}\,\mathrm{d}A\ , \tag{5}$$

where A is the area of the global ocean. The hydrostatic pressure corresponding to this sea level correction, which is not dynamically relevant but can be important for OAM calculations, was then added to p_b. For the rest of the manuscript, p_b denotes the corrected bottom pressure. Note that the spatial weighting factors for P_1 and P_2 in Eq. (1) are such that their integral over the global ocean would be zero for an aqua planet (see Fig. 8a in Ponte and Stammer 1999), which implies that any error in applying a homogeneous correction is bound to have less of an effect on the results presented here for L_1 and L_2 than it does for L_3.

3 Analysis of OAM

Given the short span of most of the records previously analyzed, very little is known about variability in OAM at interannual and longer periods, including possible interannual changes in the annual cycle. The 240-year time series of OAM for the control and forced runs, shown in Figs. 1 and 2, respectively, are analyzed here with the purposes of characterizing the OAM signals, from seasonal to multidecadal periods, associated with natural climate variability and searching for possible signatures in OAM of anthropogenically forced climate signals, including possible long term trends. The anthropogenic signals are established by examining differences between the forced and control runs. Note, however, that some of these differences can also be due to natural variability of the model (e.g., natural, very low-frequency oscillations may look like long-term trends), and that for a more definite separation of natural and anthropogenic climate signals ensemble averaging analysis would be needed. These considerations should be kept in mind when interpreting the results. In what follows, we focus first on the long term trends and then on other time scales.

3.1 Long term trends

The search for long term trends is a common focus of climate analysis. Assessing trends in ocean models is, however, made difficult by the usual presence of spurious drifts, particularly in the density fields. To mitigate the effects of any spurious signals, one can focus on the difference between trends in control and forced cases and examine only any potential trends in OAM owing to anthropogenic forcing effects. We follow this approach here with the implicit assumption that the processes responsible for the differences in control and forced trends combine linearly (i.e., differences between forced and control runs are independent of the control drift).

Of the OAM components in Figs. 1 and 2, trends in V_1, P_2, and V_2 seem negligible, while P_1 does show a trend but similar in both control and forced runs. In contrast, V_3 has an upward trend in the forced run not present in the control case. Similarly, P_3 shows a negative trend in the control run but is relatively constant in the forced run, which implies an increase in P_3 in the latter case of size similar to the control drift. In this interpretation, anthropogenic climate forcing leads to long term increases in both P_3 and V_3, and consequently L_3, although we note that the signal in P_3 is not large compared to possible systematic model errors.

To gain insight into the trends in P_3 and V_3, the regional trends of the fundamental variables, zonal velocity and bottom pressure, were investigated. Linear least-square trends were fit to p_ρ, p_s, p_b ($= p_\rho + p_s +$ sea level correction), and u at each grid point for the control and the forced runs, and the former were subtracted from the latter to determine the climate signal (Figs. 3 and 4).

Trends of p_ρ in Fig. 3a are mostly negative and indicate the influence of heat uptake, with the ocean

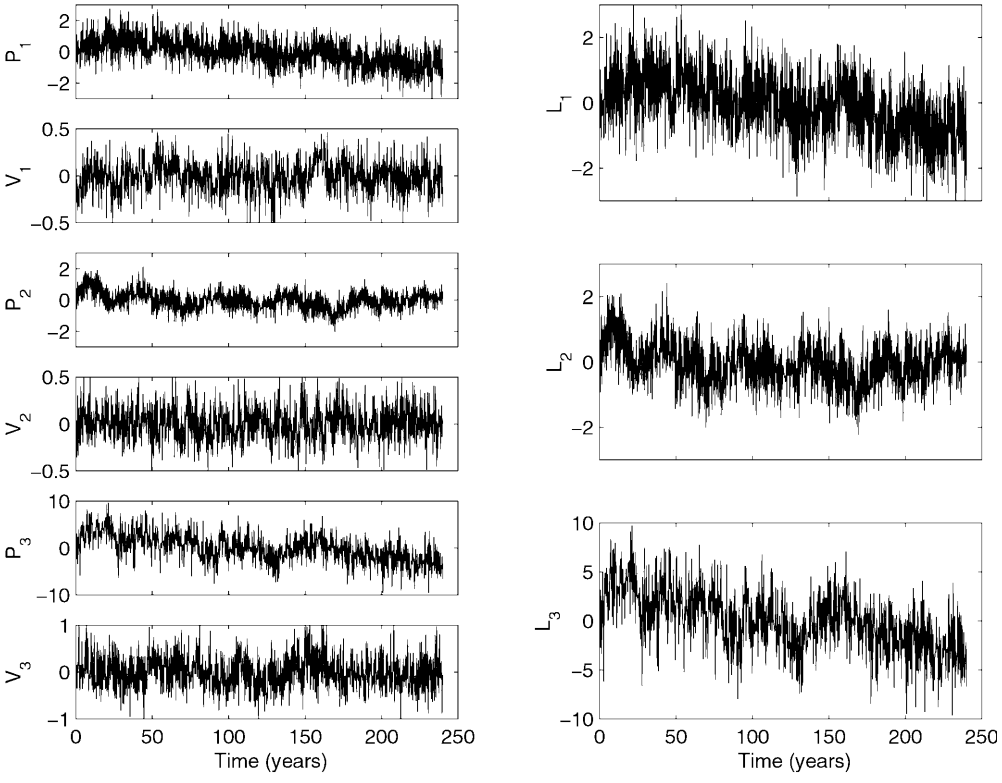

Fig. 1. Time series of P and V components (*left panels*) and total OAM (*right panels*) along the three axis for the control run. The units on all y-axes are $\times 10^{24}$ kg m^{2}s^{-1}

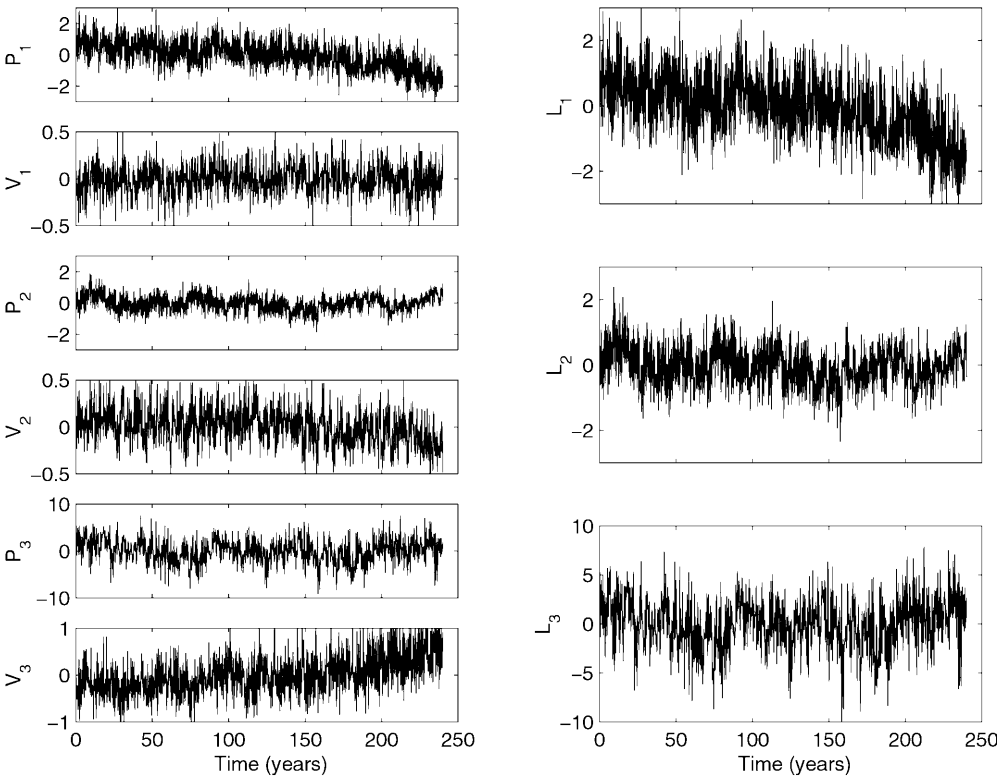

Fig. 2. Same as Fig. 1, but for the forced run

absorbing heat at most latitudes but certainly not in a homogeneous fashion (Gregory 2000). The decreases in p_ρ seem on average stronger in the Pacific than in other basins, and also weaker near Antarctica and in some shallow areas. Patterns in p_s trends are closely linked to those in p_ρ and partially compensate for spatial gradients in p_ρ trends (Fig. 3b). (Note that the relation between p_s and p_ρ is not simply a direct result of thermal effects but reflects interactions among thermal forcing, pressure gradients, and ocean currents and mass transports in the model.) As a result of this cancellation, local trends in p_b (Fig. 3c) are substantially weaker and spatially much more homogeneous and reveal a shift of mass from the Pacific to the Indian and South Atlantic Ocean and also from deep ocean to shallow coastal regions and the Arctic in general. Both patterns are consistent with the warming signals discussed in Fig. 3a and reflect the importance of volume effects on the determination of trends in L_3. Inhomogeneous warming can lead to mass shifts away from regions where warming effects are larger. Averaged p_b trends at each latitude (not shown) indicate a long-term equatorward transfer of mass consistent with the increase noted in P_3.

Interpretation of the long-term trend in V_3 is comparatively more straightforward. Local zonal velocity trends in Fig. 4 show a banded character in latitude, with negative values over ~40°–60°N and ~20–40°S and mostly positive values elsewhere on average, including a clear spin up of the eastward Antarctic Circumpolar Current (ACC). The contributions from increasing eastward and westward flows in the tropical and gyre circulations nearly cancel out; the contribution of the ACC estimated as $2\pi r^2 \rho_o T \cos^2\phi$, where T is the ACC transport and ϕ is a representative latitude after Munk and MacDonald (1960) and Ponte and Stammer (2000), nearly explains the increase in V_3. The ACC transport increases from 215 Sv to 225 Sv over the 240 years of the forced run, contributing an OAM change of about 6.4×10^{23} kg m^2 s^{-1}, which is nearly all the increase in V_3 during the forced run (Fig. 2). The trends in u are likely related to wind curl forcing trends in the coupled model and related changes in Sverdrup transports, but thermodynamic forcing trends in the ACC region are probably also relevant (e.g., Gent et al. 2001).

3.2 Variability at seasonal and longer periods

All P and V terms in Figs. 1 and 2 show a clear annual cycle superposed on interannual and longer period variability. We quantify the variability as a function of time scale by calculating the spectra of L_1, L_2 and L_3 for the forced run (Fig. 5). Results are similar for the control run (not shown), indicating that in general natural and anthropogenically-forced variability in the OAM model records are for the most part indistinguishable. The only clear periodicity in the records is the annual cycle. Apart from the annual peak, distribution of power is white or slightly red in frequency. Annual peaks are dominant in L_1 and L_2 spectra, but for L_3 the power at annual and decadal periods seems equally important. As apparent from the different amplitudes of P and V series

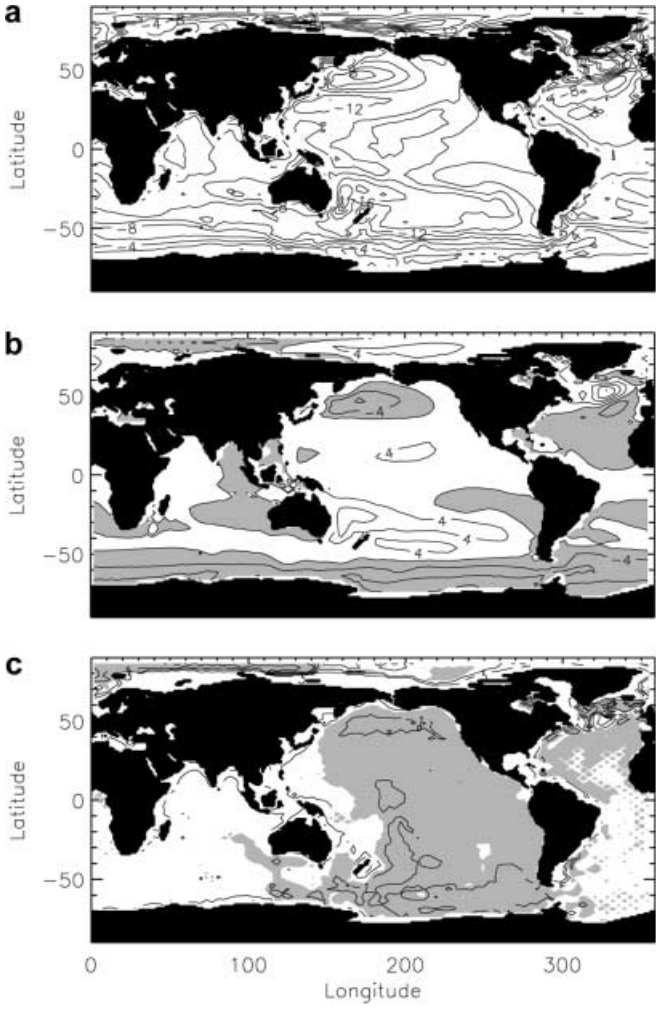

Fig. 3. Spatial distribution of the trends of **a** p_ρ, **b** p_s, and **c** p_b for the forced run, after subtracting the trends for the control run. *Light shading* in **b** and **c** denotes negative values. Units are Pa/yr and contour intervals are **a** 2 Pa/yr, **b** 4 Pa/yr, and **c** 2 Pa/yr

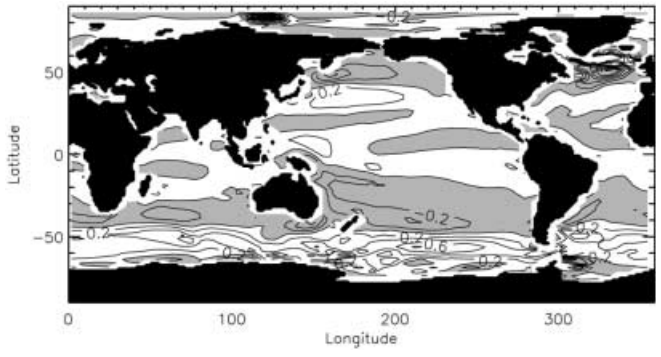

Fig. 4. Spatial distribution of the trends in depth-averaged zonal velocity of the forced run, after subtracting the trends for the control run. *Shading* denotes negative values. Units are mm s^{-1}/yr and contour interval is 0.2 mm s^{-1}/yr

in Fig. 2 and confirmed by their separate spectra (not shown), variability in P terms contribute the most to the spectra of L in Fig. 5 at most frequencies. Ponte et al.

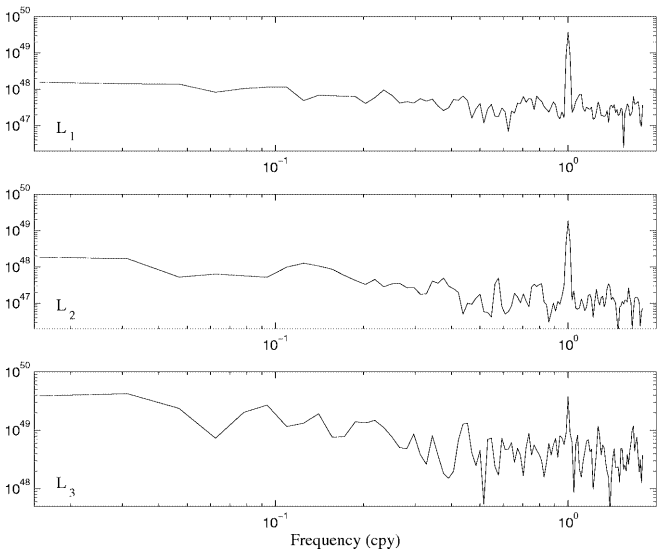

Fig. 5. Spectra of L_1 (*top*), L_2 (*center*) and L_3 (*bottom*) for the forced run. The units for all y-axes are (kg m^2 s^{-1})^2/cpy and the *first point plotted* corresponds to period of 64 years. Variance at each frequency can be obtained by multiplying the spectral value by 0.05 cpy and dividing by 2

(1998) and Ponte and Stammer (2000) found similar behavior at seasonal periods.

Spectra in Fig. 5 provide an assessment of the average OAM variability, but climate fluctuations can potentially lead to changes in OAM characteristics with time. To investigate this issue, we perform a sliding-window variance analysis over consecutive 20-year periods, after detrending OAM series within each window (Fig. 6). All OAM components show substantial changes in variance levels (∼100%) at multidecadal time scales. These changes reflect modulations in the amplitude of all variability at periods of ∼20 years and shorter, but contributions from modulation in annual cycle amplitudes are particularly important, especially for L_1 and L_2 given the dominant annual peaks in the spectra of Fig. 5. Large changes in the strength of the OAM seasonal cycle at decadal time scales are thus suggested.

Modulations in Fig. 6 have similar amplitudes in forced and control runs and are, thus, likely part of the natural variability in the model and not a result of anthropogenic forcing. There is, however, an apparent downward trend in L_2 variance in the forced run, and consistently lower variance when compared to control run in the last half of the record, when enhanced anthropogenic forcing effects are expected. Changes at the annual period are important to this behavior. Fig. 7 shows the variance associated with the annual cycle in P_2 and V_2 for the control run and for two different periods of the forced run, 1860–1990 and 1990–2100, chosen to highlight the anthropogenic forcing effects after 1990. For both P_2 and V_2, the annual cycle for the period 1990–2100 of the forced run is indeed significantly weaker than that for the earlier segment or for the control case.

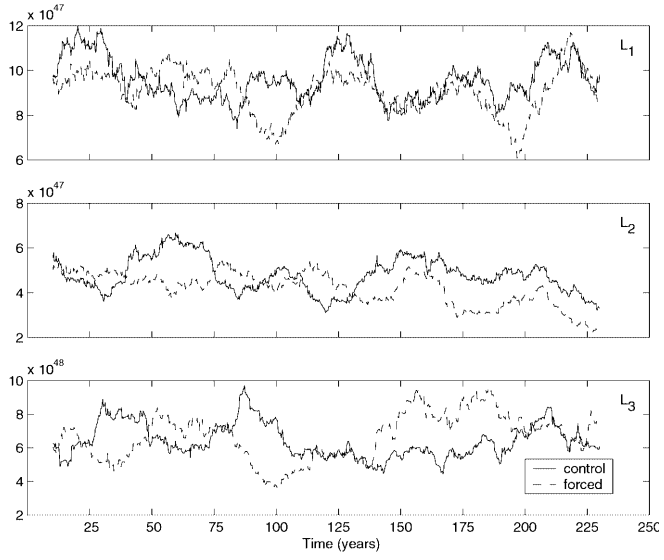

Fig. 6. Variance in a sliding 20-year window for L_1 (*top*), L_2 (*middle*), and L_3 (*bottom*), for the control and forced runs. The units on the y axes are in (kg m^{2}s^{-1})^2. Note the *different scale* for L_3. The window was slid forward one point (three months) at a time to calculate the variance at the mid-point of the window; therefore, not all points are independent

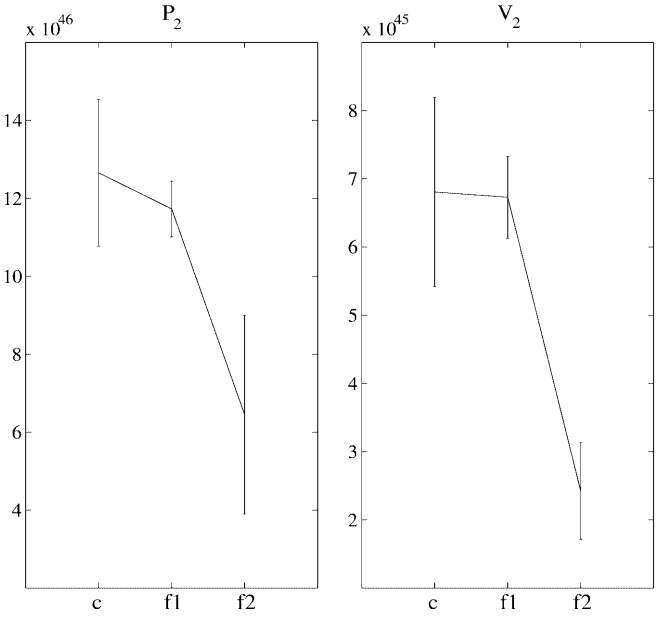

Fig. 7. The annual variance in P_2 (*left*) and V_2 (*right*) with 95% error bars for the control and forced cases labeled *f1* (1860–1990) and *f2* (1990–2100). Results are based on spectra calculated for 30-year segments, after detrending over each segment. The units for the variance on the y-axes are (kg m^{2}s^{-1})^2; notice the *different scales* in the *two panels*

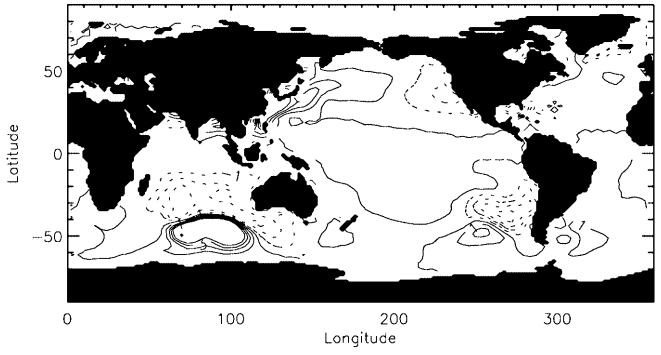

Fig. 8. Annual variances of regional P_2 values calculated at each model grid box for the last 110 years of the forced run, after subtracting the corresponding variances for the control run. *Dashed contours* denote negative values. Units are (kg m^{2}s^{-1})^2 and contour interval is 1×10^{43} (kg m^{2}s^{-1})^2. *Largest contour* plotted is 4×10^{43} (kg m^{2}s^{-1})^2

Amplitudes of P_2 are much larger than those of V_2 in Fig. 7 and thus determine the behavior of L_2. To relate the observed decrease in P_2 annual variance to changes at a regional level, we also examined the annual variances for the local integrals of P_2 over each model grid box based on the last 110 years. Fig. 8 shows the difference in these regional annual variances between forced and control runs. Because phase information is lost in these calculations, regions of increased variance in Fig. 8 may actually lead to a decrease in global P_2 variance or vice-versa, depending on the phase relation between local and global annual cycles. Thus, the sign of the differences in Fig. 8 is not important, only the amplitudes. Largest changes in annual variance occur in regions such as the southeastern Pacific and the southern Indian Ocean and the western North Pacific that are known to contribute strongly to the annual variability in L_2, as discussed by Ponte and Stammer (1999). The regions in the Southern Hemisphere show a dipole pattern (Fig. 8) suggesting shifts in the spatial position of the regional peaks of annual P_2 variance between control and forced cases. All changes in P_2 are ultimately caused by seasonal variability in bottom pressure. Changes highlighted in Fig. 8 are likely related to climate fluctuations in surface wind curl patterns, judging from current understanding of seasonal bottom pressure dynamics (Ponte 1999).

4 OAM signals and Earth rotation

As discussed in the Introduction, variability in OAM can excite signals in PM and LOD. The study of such interactions is generally carried out using excitation functions χ (e.g., Barnes et al. 1983), which represent the effective driving of Earth rotation signals by geophysical processes. Following Barnes et al. (1983), the relation between (nondimensional) χ and L quantities is simply given by

$$(\chi_1^P, \chi_2^P) = \frac{1.0}{\Omega(C-A)}(P_1, P_2)$$

$$(\chi_1^V, \chi_2^V) = \frac{1.43}{\Omega(C-A)}(V_1, V_2)$$

$$(\chi_3^P, \chi_3^V) = \frac{(0.7, 1.0)}{\Omega C}(P_3, V_3)$$

where C and A are the polar and equatorial moments of inertia of the mantle, and the numerical factors 1.0, 1.43, and 0.7 account for the rotational and surface-loading deformation effects.

The OAM time series were used to compute the pressure (χ^P) and velocity (χ^V) functions, with total excitation along any one axis given by $\chi^P + \chi^V$. Using these χ series, we reexamine the role of OAM in the excitation of PM at annual, Chandler, and longer periods, and of LOD changes. Discussion focuses on the forced run; control run results are reported when warranted by differences with the forced run. Some of the PM analyses follow closely those of Celaya et al. (1999) to facilitate comparison with their results. The reader is referred to Celaya et al. (1999), Barnes et al. (1983), and references therein for details on the derivation of the χ functions and their relation to PM and LOD.

4.1 Annual wobble

A major signal in observed PM is the prograde annual wobble. To estimate the average oceanic excitation of this wobble in our 240-year climate series, and for comparison with previous results, the phase θ and amplitude A of the annual prograde component of $\chi_1 + i\chi_2$, as well as ${\chi_1}^P + i{\chi_2}^P$ and ${\chi_1}^V + i{\chi_2}^V$, were determined for twelve consecutive 20-year segments and averaged together (Table 1). Our estimate of A for χ is in good agreement with that of Celaya et al. (1999), obtained with a different climate model. There are, however, noticeable differences between χ^P and χ^V values in the two climate models, with larger amplitudes found in Celaya et al. (1999), particularly for χ^V, and also substantially different phases in general. In our case, the amplitude of χ^P is ~5 times that of χ^V, whereas in Celaya et al. this ratio is only ~2. These differences apparently cancel out when calculating total χ. Amplitudes of χ are also similar (within a factor of 2 or 3) to those calculated by Wahr (1983) and Ponte and Stammer (1999), despite the totally different nature of the latter models.

The prograde annual power was also estimated in a sliding 20-year window, following the same procedure as in Fig. 6, to examine its interannual variability. Results in Fig. 9 show large interannual modulations (~100%) at decadal and longer time scales, with dominant contributions from χ^P. Although the annual cycle in χ_2 in the second half of the forced run was significantly lower than that in the first half, as can be inferred from Fig. 7, the prograde annual wobble excitation (which depends on both χ_1 and χ_2 and their relative amplitudes and phases) does not show such a difference in Fig. 9. Thus, no discernable anthropogenic signal in prograde annual wobble driving is found in HadCM2, although significant natural climate variability is suggested.

Given the results in Fig. 9, the differences in various estimates of annual prograde power in Table 1 are not surprising and may result not only from the different models used but also the particular periods studied. The averaged oceanic excitation based on HadCM2 results can account for nearly one fourth of the averaged observed annual wobble excitation (~0.72–0.88 × 10^{-7} rad according to Gross 2000b). Thus, our results confirm the important role of OAM to the annual wobble excitation found by Ponte et al. (1998), Ponte and Stammer (1999), and Celaya et al. (1999), and at the same time indicate the potential for significant variations in that role from year to year.

Table 1. Annual prograde excitation: (A, θ) are to be interpreted as $A\cos(\omega t + \theta)$, with $\theta = 0$ corresponding to Jan 1, where A is in 10^{-7} rad and θ is in degrees. Note that because data points in time series are spaced three months apart, the inherent uncertainty in the phase is approximately ±45°. Values of (A, θ) from Ponte and Stammer (1999), Celaya et al. (1999), and Wahr (1983) are tabulated for comparison under PS, C, and W, respectively

	HadCM2	PS	C	W
χ	0.19, 126°	0.335, 65°	0.14–0.22, 13°–32°	0.07, –83°
χ^P	0.19, 134°		0.38–0.42, –8°–1°	
χ^V	0.03, 51°		0.21–0.26, 160°–177°	

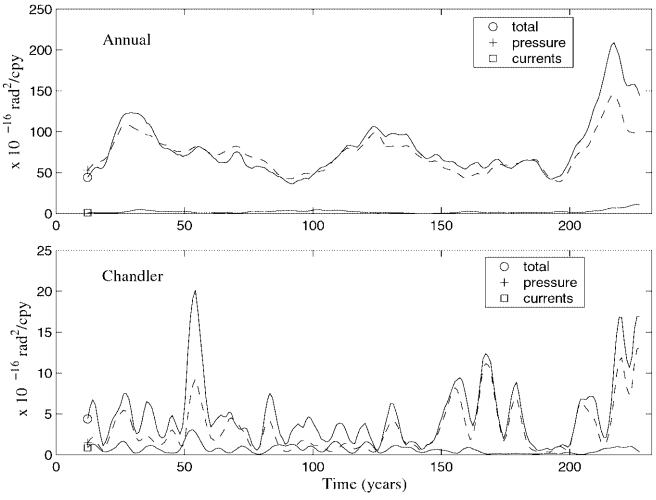

Fig. 9. Sliding window estimate of polar motion excitation by χ^P (*dashed line*), χ^V and total χ at the prograde annual (*top*) and Chandler (*bottom*) frequencies, using output from the forced run

4.2 Chandler wobble

The prograde Chandler wobble corresponds to a free mode of the Earth at ~14 months and is the largest PM signal in the observations. The average Chandler prograde power, taken here as the average power over three harmonics (0.8, 0.85, and 0.9 cpy) as in Celaya et al. (1999), and its interannual variability were estimated as done for the annual cycle, after removing the annual harmonic from the oceanic χ series. Average power amplitudes are given in Table 2, together with similar estimates based on Ponte and Stammer (1999) and Gross (2000a) for comparison, and interannual modulations of that power are shown in Fig. 9.

Table 2. Amplitude ($\times 10^{-8}$) of Chandler excitation averaged over harmonics 0.8, 0.85 and 0.9 cpy. Ponte and Stammer (1999) values are based on a single harmonic at 0.84 cpy. Original estimates from Gross (2000a) contained the integrated power over three harmonics, 0.73, 0.82, and 0.91 cpy, and have been divided by three for consistency here

	HadCM2	Ponte and Stammer (1999)	Gross (2000a)
χ	0.23	0.23	0.31
χ^P	0.19		0.30
χ^V	0.08		0.06

Average Chandler power estimates in Table 2 are remarkably similar to previous values, although the contribution of χ^V seems larger in HadCM2 results than in those reported by Gross (2000a). The relative role of χ^V and χ^P seems to depend significantly on the period considered (Fig. 9). Large oceanic excitation is usually related to χ^P variability, but χ^V can be equally important over periods of weaker power (e.g., between 90 and 130 years in Fig. 9). In general, there is large (greater than 100%) interannual variability for χ over decadal and longer time scales, but with significantly more modulation at shorter scales than seen for the annual wobble excitation, reflecting the more random nature of variability over the Chandler band.

Most importantly, the HadCM2 oceanic Chandler excitation power in Fig. 9 is similar in mean magnitude and interannual variations to the observed mean geodetic excitation power between 0.8 and 0.9 cpy reported by Celaya et al. (1999). Our results thus confirm the major role of the ocean in driving the Chandler wobble. In addition, as for the annual wobble, although anthropogenic climate signals were not detected in comparisons between forced and control runs, natural climate variability should lead to large modulations in oceanic power available to drive the Chandler wobble.

4.3 Low frequency PM

Interannual PM signals are generally weak but contain a clear oscillation called the Markowitz wobble at periods of ~20–30 years. Celaya et al. (1999) investigated the possible role of OAM climate signals as a source of the Markowitz wobble and found typical excitation amplitudes to be too small by a factor of 2 and with apparently longer periods. Following Celaya et al. (1999), we examine the oceanic excitation at low frequencies by smoothing original χ_1, χ_2 series using a sliding Gaussian window with a decay constant of five years. Prior to this smoothing, the annual harmonic is removed and the control trends are subtracted from the forced χ functions to remove any model drift.

Smoothed χ series are shown in Fig. 10, together with corresponding trace of the low frequency wobble at the pole. This trace describes the actual motion of the pole of rotation that would occur under the calculated oceanic excitation and is determined by solving a simple ordinary differential equation relating χ_1, χ_2 to PM, as described in detail by Celaya et al. (1999) or Barnes et al. (1983). The low frequency HadCM2 χ series show variations at 20–30 years and at longer time scales, with pressure effects dominating. Variability at the Markowitz time scale is much more evident in our results than in those of Celaya et al. (1999), but PM amplitudes are $\sim 2 \times 10^{-8}$ rad, which is only about one fourth of the observed amplitudes. In addition, the PM trace does not exhibit any clear preferred direction as observed in the data (Celaya et al. 1999). These results suggest that the ocean can contribute to the Markowitz wobble but that other geophysical processes are most likely also involved.

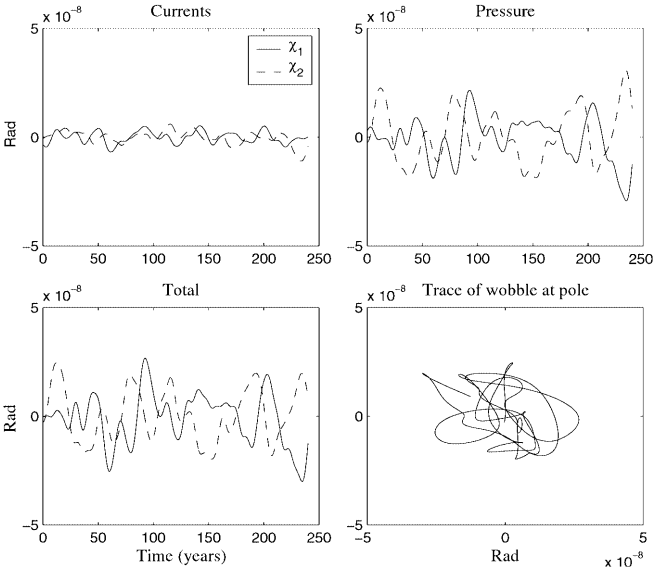

Fig. 10. Smoothed polar motion excitation by the currents (*top left*), pressure (*top right*), and the total ocean (*bottom left*) at low frequencies. *Solid line* represents χ_1 and *dashed line* χ_2. Trace of the wobble at the pole, representing the motion of the pole of rotation driven by the total ocean excitation, is shown in the *bottom right panel*

4.4 Effects on LOD

Although the impact of OAM on LOD fluctuations is expected to be small judging from studies of the seasonal cycle (e.g., Marcus et al. 1998; Ponte and Stammer 2000), behavior at longer periods has not been quantitatively examined. Our results yield an annual cycle in χ_3 with an amplitude of $\sim 1.9 \times 10^{-10}$ rad or equivalent to an LOD signal of 16 μsec, with the maximum occurring around mid August (±45 days). The inferred amplitude and phase are in good agreement with previous estimates (e.g., Marcus et al. 1998; Ponte and Stammer 2000) and correspond to ~5% of the annual change in LOD.

The low-frequency excitation, obtained by smoothing 3-monthly series over 8 points to eliminate the seasonal

cycle, is examined in Fig. 11 for the forced run. Range of variability is $\sim 10^{-9}$, which is equivalent to LOD changes of < 0.1 ms. Similar amplitudes are expected from long term trend effects. (These signals are related to differences between control and forced trends and thus not readily inferred from Fig. 11, but note that variability in the forced L_3 series in Fig. 2 is similar to the control trend in L_3 in Fig. 1.) For comparison, effects of tidal braking produce a secular trend on LOD of more than 2 ms/century (Eubanks 1993) and changes in AAM estimated in global warming scenarios amount to $\sim$0.5 ms/century (Huang et al. 2001). Oceanic perturbations on LOD are certainly small at the longest scales, but not totally negligible at interannual periods given observed variability in LOD on the order of 1 ms (e.g., Hide and Dickey 1991; Abarca del Rio et al. 2000).

5 Summary and discussion

Based on the HadCM2 climate runs analyzed, natural climate fluctuations are expected to induce large changes in OAM variability, particularly in the strength of its seasonal cycle, which can be modulated at decadal and longer time scales. Besides the annual cycle, no other mode of variability is readily distinguishable in OAM. In particular, although the HadCM2 simulates quite well variability associated with El Niño-Southern Oscillation events (Collins 2000), such variability does not seem to produce discernable spectral signatures in OAM. The seasonal and longer period OAM signals simulated by HadCM2 are largely related to variability in bottom pressure and are found to be potentially important sources of PM at annual, Chandler, and Markowitz periods.

Large anthropogenically forced signals in OAM are not detected in HadCM2 runs but there is an increasing trend in L_3, associated with inhomogeneous warming trends and corresponding mass shifts towards low latitudes, and also to a lesser extent with a spin up of the ACC and eastward transports in the Southern Ocean. In addition, a marked decrease in the annual cycle in L_2, related to changes in seasonal bottom pressure and currents in North Pacific and Southern Ocean regions, is also predicted for the period after 1990. Impact of these signals on Earth spin rate and wobble are, however, expected to be weak compared to other geodetic signals.

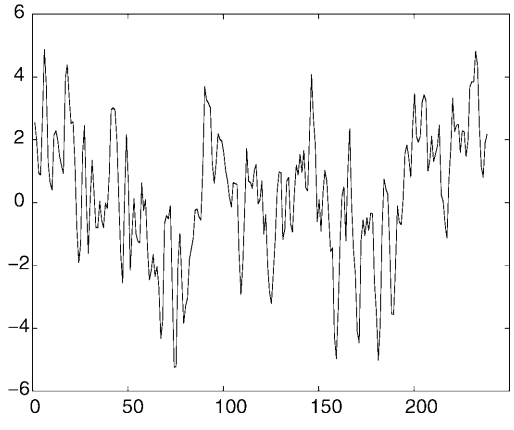

Fig. 11. Smoothed time series of χ_3 for the forced run. Smoothing was done by averaging every eight points. Units are years for x-axis and $\times 10^{-10}$rad for the y-axis

Our approximate treatment of non-Boussinesq effects (i.e., expansion and contraction of water parcels and corresponding changes in volume) points to their potential importance when determining OAM signals at long (climate) time scales, particularly for L_3. Warming or cooling patterns with spatial variations do not change the total ocean mass but can lead to significant redistribution of mass globally and thus to OAM changes. The ability of ocean models to explicitly represent non-Boussinesq effects may thus be an important asset when seeking the most accurate representation of the variability in the oceanic mass field.

Mass fluxes related to hydrological effects (runoff, precipitation, ice melting, etc.) can lead to eustatic sea level signals and thus to changes in OAM. Although these signals are not explicitly calculated in the rigid lid model and thus not treated here, we note that hydrological effects may be important for the Earth rotation problem (e.g., Celaya et al. 1999). In this regard, related OAM changes are directly tied to mass transfers from land and glaciers and are best treated in the context of the global hydrological cycle, which is beyond our scope.

Natural and anthropogenic climate signals highlighted in OAM reflect variability in major ocean current systems (e.g., ACC, gyre circulation in North Pacific, etc.) and correlated patterns in p_b, or nonuniform rise in temperature. Thus, OAM can be used as a global index of the ocean climate state. As a measure of the vertically integrated horizontal circulation, OAM can serve as a useful complement to more traditional measures of ocean climate such as the strength of the meridional overturning circulation. In addition, OAM provides a unique global measure of the oceanic mass field. Any such use of OAM must of course be tempered by the fact that important regional OAM signals, as seen for example for the case of V_3 discussed in Fig. 4, can cancel out leaving no discernible signal in the global values. Besides providing insight on climate signals in ocean circulation and mass fields, studies of OAM in the context of the planet's angular momentum budget, as attempted here, are also another way of checking behavior in climate models against independent geodetic data that represent the integrated effects of the global climate system.

Acknowledgements We thank P. Nelson for helping with initial data transfer and setup and R. Rosen and two anonymous reviewers for useful comments on the manuscript. Work at AER was supported by the NASA Solid Earth and Natural Hazards Program (contract NAS-97270) and the EOS Project (grant NAG5-9989). Work at the Hadley Centre was supported by the UK Department of the Environment, Transport and the Regions under contract PECD 7/12/37 and the Public Meteorological Service Research and Development Programme.

References

Abarca del Rio R, Gambis D, Salstein DA (2000) Interannual signals in length of day and atmospheric angular momentum. Ann Geophys 18: 347–364

Barnes RTH, Hide R, White AA, Wilson CA (1983) Atmospheric angular momentum fluctuations, length-of-day changes and polar motion. Proc R Soc London A 387: 31–73

Brzeziński A, Nastula J (2001) Investigation of the oceanic excitation of non-seasonal polar motion. Adv Space Res (in press)

Celaya MA, Wahr JM, Bryan FO (1999) Climate-driven polar motion. J Geophys Res 104: 12,813–12,829

Chao BF, Zhou YH (1999) Meteorological excitation of interannual polar motion by the North Atlantic Oscillation. J Geodyn 27: 61–73

Collins M (2000) The El Niño-Southern Oscillation in the second Hadley Centre coupled model and its response to greenhouse warming. J Clim 13: 1299–1312

Eubanks TM (1993) Variations in the orientation of the Earth. In: Smith D, Turcotte D, (eds.) Contributions of Space Geodesy to Geodynamics: Earth Dynamics, American Geophysical Union Monograph, Geodynamics Series 24, pp 1–54

Gent PR, Large WG, Bryan FO (2001) What sets the mean transport through Drake Passage? J Geophys Res 106: 2693–2712

Greatbatch RJ (1994) A note on the representation of steric sea level in models that conserve volume rather than mass. J Geophys Res 99: 12,767–12,771

Gregory JM (1993) Sea level changes under increasing atmospheric CO_2 in a transient coupled ocean–atmosphere GCM experiment. J Clim 6: 2247–2262

Gregory JM (2000) Vertical heat transports in the ocean and their effect on time-dependent climate change. Clim Dyn 16: 501–515

Gregory JM, Lowe J (2000) Predictions of global and regional sea-level rise using AOGCMs with and without flux adjustment. Geophys Res Lett 27: 3069–3072

Gross RS (2000a) The excitation of the Chandler wobble. Geophys Res Lett 27: 2329–2332

Gross RS (2000b) Combinations of Earth orientation measurements: SPACE97, COMB97, and POLE97. J Geodesy 73: 627–637

Hide R, Dickey JO (1991) Earth's variable rotation. Science 253: 629–637

Hide R, Dickey JO, Marcus SL, Rosen RD, Salstein DA (1997) Atmospheric angular momentum fluctuations during 1979–1988 simulated by global circulation models. J Geophys Res 102: 16,423–16,438

Houghton JT, Callender BA, Varney SK (eds) (1992) Climate change 1992. The supplementary report to the IPCC scientific assessment. WMO-UNEP, Cambridge University Press, Cambridge, UK, pp 200

Huang H-P, Weickmann KM, Hsu CJ (2001) Trend in atmospheric angular momentum in a transient climate change simulation with greenhouse gas and aerosol forcing. J Clim 14: 1525–1534

Johns TC, Carnell RE, Crossley JF, Gregory JM, Mitchell JFB, Senior CA, Tett SFB, Wood RA (1997) The second Hadley Centre coupled ocean-atmosphere GCM: model description, spinup and validation. Clim Dyn 13: 103–134

Lambeck K (1980) The Earth's variable rotation. Cambridge University Press, Cambridge, UK, pp 449

Marcus SL, Chao Y, Dickey JO, Gegout P (1998) Detection and modeling of nontidal oceanic effects on Earth's rotation rate. Science 281: 1656–1659

Mitchell JFB, Johns TC, Gregory JM, Tett SFB (1995) Climate response to increasing levels of greenhouse gases and sulphate aerosols. Nature 376: 501–504

Munk WH, MacDonald GJF (1960) The rotation of the Earth. Cambridge University Press, Cambridge, UK, pp 323

Ponte RM (1999) A preliminary model study of the large-scale seasonal cycle in bottom pressure over the global ocean. J Geophys Res 104: 1289–1300

Ponte RM, Stammer D (1999) Role of ocean currents and bottom pressure variability on seasonal polar motion. J Geophys Res 104: 23,393–23,409

Ponte RM, Stammer D (2000) Global and regional axial ocean angular momentum signals and length-of-day variations (1985–1996). J Geophys Res 105: 17,161–17,171

Ponte RM, Stammer D, Marshall J (1998) Oceanic signals in observed motions of the Earth's pole of rotation. Nature 391: 476–479

Rosen RD (1993) The axial momentum balance of Earth and its fluid envelope. Surv Geophys 14: 1–29

Rosen RD, Gutowski Jr WJ (1992) Response of zonal winds and atmospheric angular momentum to a doubling of CO_2. J Clim 5: 1391–1404

Rosen RD, Salstein DA (2000) Multidecadal signals in the interannual variability of the atmospheric angular momentum. Clim Dyn 16: 693–700

Rosen RD, Salstein DA, Eubanks TM, Dickey JO, Steppe JA (1984) An El Niño signal in atmospheric angular momentum and Earth rotation. Science 225: 411–414

Salstein DA, Rosen RD (1986) Earth rotation as a proxy for interannual variability in atmospheric circulation, 1860-present. J Clim Appl Meteorol 25: 1870–1877

Tett SFB, Johns TC, Mitchell JFB (1997) Global and regional variability in a coupled AOGCM. Clim Dyn 13: 303–323

Wahr JM (1983) The effects of the atmosphere and oceans on the Earth's wobble and on the seasonal variation in the length of day – II. Results. Geophys J R Astr Soc 74: 451–487

Wünsch J (2000) Oceanic influence on the annual polar motion. J Geodyn 30: 389–399